HHS Public Access

Author manuscript

Biochemistry. Author manuscript; available in PMC 2019 March 20.

Published in final edited form as:

Biochemistry. 2018 March 20; 57(11): 1702–1710. doi:10.1021/acs.biochem.7b01075.

Tuning Inner-Ear Tip-Link Affinity Through Alternatively Spliced Variants of Protocadherin-15

Yoshie Narui and **Marcos Sotomayor***

The Ohio State University, Department of Chemistry and Biochemistry, Columbus, Ohio 43210

Abstract

Human hearing relies upon the tip-to-tip interaction of two non-classical cadherins, protocadherin-15 (PCDH15) and cadherin-23 (CDH23). Together, these proteins form a filament called the tip link that connects neighboring stereocilia of mechanosensitive hair cells. As sound waves enter the cochlea, the stereocilia deflect and tension is applied to the tip link opening nearby transduction channels. Disruption of the tip link by loud sound or calcium chelators eliminates transduction currents and illustrates that tip-link integrity is critical for mechanosensing. Tip-link remodeling after disruption is a dynamic process, which can lead to the formation of atypical complexes that incorporate alternatively spliced variants of PCDH15. These variants are categorized into 6 groups (N1-N6) based upon differences in the first two extracellular cadherin (EC) repeats. Here, we characterized the two N-terminal EC repeats of all PCDH15 variants (pcdh15(N1) to pcdh15(N6)), and combined these variants to test complex formation. We solved the crystal structure of a new complex composed of CDH23 EC1-2 (cdh23) and pcdh15(N2) at 2.3 Å resolution and compared it to the canonical cdh23-pcdh15(N1) complex. While there were subtle structural differences, the binding affinity between cdh23 and pcdh15(N2) is ~6 times weaker than cdh23 and pcdh15(N1) as determined by surface plasmon resonance analysis. Steered molecular dynamics simulations predict that the unbinding force of the cdh23-pcdh15(N2) complex can be lower than the canonical tip link. Our results demonstrate that alternative heterophilic tip-link structures form stable protein-protein interactions *in vitro* and suggest that homophilic PCDH15-PCDH15 tip links form through the interaction of additional EC repeats.

INTRODUCTION

At the molecular level, human hearing relies upon the tip-to-tip interaction of two unique non-classical cadherins, protocadherin-15 (PCDH15) and cadherin-23 (CDH23).[1–5] Together, these two proteins form a filament called the tip link that connects adjacent stereocilia of mechanosensitive hair cells.[6, 7] Sound waves cause the stereocilia to deflect applying tension to the tip link and opening a nearby transduction channel.[8, 9] Disruption of the tip link caused by loud sound or chemical treatments eliminates transduction currents and illustrates that tip-link integrity is critical for mechanosensing.[10–13]

*Corresponding Author: sotomayor.8@osu.edu. Phone: (614) 688-2070.

Supporting Information. Full details of protein sequences and purification, validation of complex formation, MALS and analytical SEC analysis, and summary of SMD simulations

The proteins forming the tip link were first identified through genetic analysis that associated PCDH15 and CDH23 with inherited forms of deafness.[14–17] Subsequent immunohistochemistry experiments showed that the lower portion of the tip link consists of a parallel dimer of PCDH15 while the upper portion is a parallel dimer of CDH23 (Figure 1A, B).[3] Similar to classical cadherins,[18, 19] the interaction between PCDH15 and CDH23 requires calcium, however, their domain structure and mode of interaction is significantly different. PCDH15 and CDH23 are exceptionally long cadherins with 11 and 27 extracellular cadherin (EC) repeats, respectively, and their predicted end-to-end length is consistent with the overall size of the tip link (~170 nm) as observed by electron microscopy.[6, 7, 20, 21] The first two N-terminal EC repeats of each protein interact to form the link between PCDH15 and CDH23 (Figure 1B). Recently, the crystal structure of this bond revealed an overlapped, antiparallel heterodimer noted for its high mechanical strength.[22] The essential relevance in inner-ear mechanotransduction of the bond revealed by this structure has been validated both *in vitro* and *in vivo*.[22, 23]

Proper formation of the tip link is necessary to transduce mechanical stimuli from sound into an electrical response. When calcium ions are removed with a chelator, BAPTA, the tip link is disrupted and transduction currents are eliminated.[10] Tip-link formation is a dynamic and reversible process.[11] Following BAPTA treatment, which mimics sound-induced damage, tip links regenerate within 24 to 36 hours. Intriguingly, a recent study observed the formation of an atypical tip link containing only PCDH15 during regeneration.[12] These links were observed in mouse inner-ear hair cells, but such interactions have never been observed *in vitro*. After 36 hours, tip links matured and returned to canonical CDH23-PCDH15 linkages (Figure 1A). While both types of tip links were able to mediate transduction currents, differences in the calcium-dependent decay of the transduction current were observed. These experiments highlight the fact that there is still much to be learned about how tip links form and regenerate and how they convert mechanical forces into biochemical signals.

PCDH15 and CDH23 are also found in alternative linkages within the hair cell bundle. Early in the development of outer hair cells, PCDH15 and CDH23 form lateral links that connect stereocilia in different rows together.[24] As hair cells mature, these proteins form connections between the kinocilium and the tallest stereocilium known as kinocilial links.[25] These alternative links play an important role in maintaining the shape and organization of the bundle and ensure that it behaves as a cohesive unit in response to an applied force. Immunostaining of hair cells suggest that variants of PCDH15, generated by alternative splicing of the genes, are located in different parts of the hair-cell bundle and may form noncanonical alternative linkages with potential biological function. However, these localization studies and further genetic analyses only focused on splice variants of the PCDH15 cytoplasmic domain (labeled CD1, CD2, and CD3) that may function redundantly.[2, 26, 27]

Identifying N-terminal splice variants of PCDH15 *in vivo* remains a challenge because current antibodies are only able to distinguish among cytoplasmic domain variants. Genetic studies suggest that PCDH15 is present in hair cells as one of at least 26 variants,[2] which may feature distinct extracellular domains that bind with either another variant of PCDH15 or with CDH23 to form noncanonical tip links. While CDH23 exists in at least 11 variant

forms, only four of them, all featuring a canonical CDH23 tip, are long enough to form tip links. This study includes all possible PCDH15 variants that have unique modifications in their first two EC repeats expected to directly interact with CDH23 (Figure 1C). We considered all complexes formed by PCDH15 variants with two N-terminal EC repeats, pcdh15(N1) to pcdh15(N6), and the canonical CDH23 EC1-2 tip (cdh23). In addition, we tested possible pseudo-heterophilic interactions between different variants of pcdh15.

Using structural information with biophysical experiments, we have determined that subtle changes in the pcdh15 molecular structure due to alternative splicing leads to clear changes in the binding affinity of the cdh23-pcdh15 complex. In addition, steered molecular dynamics (SMD) results predict that dissociation of noncanonical complexes requires less force than that needed to unbind the canonical tip-link complex. Precisely when and where each splice variant appears in hair cells has not been determined, yet splice variants of PCDH15 are able to provide fine control of tip-link affinity and may enhance the dynamic range of its binding strength.

MATERIALS AND METHODS

Protein Expression and Purification

The gene coding for each mouse pcdh15 variant was inserted into pET21a for bacterial expression. The sequences for each variant are as follows: variant N1, residues Q27-D259 (UniProt entry Q99PJ1-1, accession no. AAG53891); variant N2, residues Q27-D254 (UniProt entry Q99PJ1-2, accession no. DQ354396); variant N3, residues Q27-D232 (UniProt entry Q99PJ1-8, accession no. DQ354402); variant N4, residues Q27-D217 (UniProt entry Q99PJ1-7, accession no. DQ354401); variant N5, residues M1-F260 (accession no. DQ354407); and variant N6, residues Q27-F254 (UniProt entry Q99PJ1-24, accession no. AAY24693; Figure S1). All constructs were sequence verified and contained a C-terminal hexahistidine tag for purification by immobilized metal affinity chromatography. Proteins were expressed in *E. coli* BL21-CodonPlus(DE3)-RIPL cells at 30°C overnight in Terrific Broth (TB) medium. Expression was induced with 0.2 mM IPTG when OD_{600} reached 0.4-0.6, except for variant N5, which was expressed at 37°C using 1 mM IPTG. All protein fragments were highly overexpressed as indicated by SDS PAGE analysis (Figure S1). The cells were pelleted at 6,000 rpm (Beckman JLA 8.1 rotor) and stored at −80°C. Because the proteins form inclusion bodies, pellets were resuspended in a denaturing lysis buffer (20 mM Tris-HCl, pH 7.5, 10 mM $CaCl_2$, 20 mM imidazole and 6 M GuHCl) and subsequently sonicated (total time 5 min, 2 s on, 5 s off, Sonix cell sonicator). The lysate solution was clarified by centrifugation for 30 min at 20,000 rpm (Beckman JA-25.50 rotor), and the clarified solution was incubated with Ni-sepharose beads on a nutator for 1 h. The beads with bound protein were rinsed 2 times with 25 mL of denaturing lysis buffer, and the protein was released with (2 × 25 mL) elution buffer (20 mM Tris-HCl, pH 7.5, 10 mM $CaCl_2$, 500 mM imidazole, 6 M GuHCl). Variants N1-N4 were then refolded through a six-step dialysis process as previously described.[22, 28] Briefly, the denatured protein sample was diluted to ~0.7 mg/mL with 2 mM DTT and dialyzed for 24 h against D buffer (20 mM Tris-HCl, pH 8.0, 10 mM $CaCl_2$) with 6 M GuHCl, followed by two additional 24 h steps of dialysis against D buffer with 3 M and 2 M GuHCl, respectively. In the final three 12 h

steps, the protein was dialyzed against D buffer with 1, 0.5, and 0 M GuHCl plus 400 mM L-arginine and 375 μM oxidized glutathione. All other variants were refolded overnight in 20 mM Tris-HCl, pH 8.0, 2 mM $CaCl_2$, 150 mM KCl, 50 mM NaCl, 400 mM L-arginine. After dialysis was complete, each variant was purified by size exclusion chromatography (SEC) on a Superdex S200 16/600 column in SEC buffer (20 mM Tris-HCl, pH 7.5, 2 mM $CaCl_2$, 150 mM KCl, 50 mM NaCl, with 2mM DTT for N5 and N6).

For surface plasmon resonance (SPR) experiments, tagless cdh23 was produced by cloning the gene (residues Q24-D228, UniProt entry Q99PF4-1) into pTXB1 (NEB, IMPACT Kit E6901S), which fuses an inducible self-cleaving intein with a chitin binding domain to the C-terminus of cdh23. CDH23 cDNA was amplified by PCR (primers: CGGCGGCTCGAGATCTCCAACTTGGATATTCACCTTCCGTGTGAT; CCGCCGGCTCTTCCGCACGCGTCCTGATGATGATGGCCAGGTTGGC) and cloned into pTXB1 using the restriction sites NdeI and SapI. An alanine residue was inserted between the end of EC2 and the intein to improve cleavage efficiency. The protein was produced in *E. coli* BL21-CodonPlus(DE3)-RIPL cells grown at 15°C overnight in lysogeny broth (LB) medium and induced with 0.4 mM IPTG when OD_{600} reached 0.4-0.6. This protein fragment was purified under native conditions by lysing cells in a native lysis buffer (column buffer: 20 mM Tris-HCl, pH 8.5, 200 mM NaCl, 1 mM $CaCl_2$, plus 0.1% (v/v) Triton X-100, 100 μM PMSF and protease inhibitor cocktail (Sigma, P8849)). Following centrifugation, the cell extract was loaded onto 10 mL of chitin beads and incubated for 90 min while inverted every 15 min. The lysate was collected and the column was washed with 20 column volumes (CVs) of column buffer to remove unbound proteins. The column was quickly washed with 3 CVs of cleavage buffer (column buffer plus 50 mM DTT). The protein was eluted with 4 CVs of cleavage buffer by stopping the flow and waiting for a minimum of 16 h at 4°C to induce self-cleavage of the intein. Finally, the protein sample was purified by SEC on a Superdex S200 16/600 column in SEC buffer.

Formation and Characterization of Tip-Link Proteins and Complexes

Each refolded variant of pcdh15 was analyzed on an AKTAmicro system (GE Healthcare Life Sciences) equipped with a Superdex 75 PC 3.2/30 column equilibrated with SEC buffer. When required, the molecular weight of constructs was determined using a miniDAWN TREOS (Wyatt) multi-angle light scattering (MALS) system placed directly in the flow path following the SEC column. To test for binding interactions between constructs, refolded protein samples were combined with a slight molar excess of cdh23 relative to pcdh15 (1.2:1). In the case where two pcdh15 variants were combined, one variant was selected to be in slight excess. The total amount of protein for each run was between 25-50 μg. The proteins were incubated together on ice for 30 min to 1 h, and the samples were inverted every 15 min. The entire sample was injected onto the analytical SEC column for analysis. All experiments were performed at 4°C using a 100 μL loop and a flow rate of 50 μL/min.

Crystallization, Data Collection, and Structure Determination

To determine the molecular architecture of the noncanonical tip-link variant complex formed by pcdh15(N2) and cdh23, its structure was solved by x-ray crystallography. Refolded and SEC purified protein fragments were prepared individually and combined in a 1.2:1 mole

ratio and incubated on ice for 30 min to 1 h. The cdh23-pcdh15(N2) mixture was repurified by SEC to isolate the complex peak for crystallization (Figure S2). Crystals of the cdh23-pcdh15(N2) complex were grown by vapor diffusion at 4°C by combining equal parts of protein (5 mg/mL) and reservoir solution containing 0.1 M HEPES, pH 7.5, 0.2 M ammonium acetate, and 25% (v/v) isopropanol. Crystals were cryoprotected with 25% glycerol and cryo-cooled in LN_2. A 2.26 Å data set was collected at the Advanced Photon Source at Argonne National Laboratory. The data set was indexed, integrated, and scaled using HKL2000,[29] and the structure was solved using molecular replacement with the canonical tip-link complex (PDB code: 4APX) as a search model in Phaser.[30] Model building was done in Coot,[31] and the refinement was completed using REFMAC5[32] applying translation-libration-screw refinement near the end of the process. Data collection and refinement statistics are listed in Table 1. Coordinates for the noncanonical tip-link complex have been deposited in the PDB with entry code 4XXW.

Surface Plasmon Resonance Analysis

SPR experiments were carried out using a Biacore T100 system and Series S NTA sensor chip (GE Healthcare). The NTA surface was activated by flowing a 0.5 mM $NiCl_2$ solution at a rate of 10 μL/min for 60 s. Next, ligand molecules, in this case, hexahistdine-tagged pcdh15 (N1 or N2) at a concentration of 1 μM, were flowed in at a rate of 10 μL/min for 30 s. The target response due to immobilized ligand was set between 500-750 RU. Once the target response was reached, the analyte, cdh23 without an affinity tag, was passed through the flow cell at 30 μL/min for 60 s. After analyte binding and dissociation was observed, the ligand was removed from the sensor surface using 500 mM imidazole applied at 30 μL/min for 90 s. This process was repeated for at least 10 different analyte concentrations ranging from 0-50 μM. Data collected from higher concentrations of cdh23 was excluded in the fitting when the response curves showed evidence of non-specific binding to the sensor surface. Following data collection, Igor Pro Software was used to determine the steady-state binding affinity.

Molecular Dynamics Simulations

With structural details, it is possible to use molecular dynamics (MD) simulations to pull on the complex until the tip link is disrupted.[33, 34] A system including the cdh23-pcdh15(N2) complex (PDB code: 4XXW, chains C and B), water molecules, and ions (150 mM KCl) was built using the VMD plug-ins psfgen, solvate and autoionize (153,825 atoms).[35] A similar system was prepared using the canonical tip-link complex (PDB code: 4AQ8; solvated chains A and C encompassing 161,038 atoms). MD simulations of these two systems were done using NAMD 2.10 and 2.11,[36] the CHARMM36 force field for proteins, and the TIP3P model for water.[37] The systems were energy-minimized and equilibrated in the constant number, pressure and temperature ensemble (*NpT*), and the resulting states were used as the starting point for SMD simulations. Two independent sets of simulations were completed for each system as summarized in Table S1. All simulations were completed at $T = 300$ K. Constant-velocity stretching simulations used the SMD method and NAMD Tcl Forces interface.[22, 38] Specifically, C_α atoms at the C-terminus of pcdh15 (N1 or N2) and cdh23 were attached to independent virtual springs of stiffness $k = 1$ kcal mol^{-1} Å^{-2}.

The stretching direction was set to be the *x*-axis matching the vector connecting the C-termini of the proteins. Maximum force peaks were computed from 50 ps running averages.

RESULTS AND DISCUSSION

The splice variants of PCDH15 can be categorized into 6 unique groups based upon the sequences of their first two EC repeats (Figure 1C). All PCDH15 splice variants (N1-N6) were produced and tested to systematically explore their properties, alone and in complex with cdh23 or other variants.

Analysis of Individual pcdh15 Variants

When individual fragments were analyzed by analytical SEC, each species appeared as a single peak representing a homogenous, properly folded protein sample (Figure 2A). Variant N3 could not be refolded and therefore, was excluded from this analysis. The retention volumes of N1 (1.22 mL), N2 (1.22 mL), N4 (1.14 mL), N5 (1.11 mL), N6 (1.18 mL), and cdh23 (1.19 mL) indicate that these samples are predominantly present as monomers in solution (Figure S4C). Variant N4 is unstable and aggregates when concentrated resulting in the appearance of a second peak near the void volume (0.87 mL). Compared with the other variants, N5 has a lower retention volume of 1.11 mL indicating a possible homodimer, but when further analyzed by MALS this splice variant of PCDH15 was determined to be a monomer (Figure S3). It should be noted that under non-reducing conditions variants N5 and N6 are present as both monomer and dimer (data not shown). Both N5 and N6 contain a single cysteine residue, which forms an intermolecular disulfide bond. These results suggest that strict homophilic dimerization of PCDH15 isoforms requires additional EC repeats or a non-reducing environment, if at all possible.

Heterophilic Complexes of pcdh15 Variants

When combined in solution, cdh23 and pcdh15(N1) come together to form the canonical tip-link complex, and the newly formed peak at 1.09 mL represents one molecule of cdh23 bound to one molecule of pcdh15(N1) (Figure 2B, green). Similarly, when pcdh15(N2) is mixed with cdh23 the proteins bind and form a heterophilic complex peak at 1.12 mL (Figure 2B, blue). This association is different from the canonical tip-link interaction as indicated by a shift in the complex peak to a higher retention volume. To complete the analysis, pcdh15 variants N5 and N6 were also combined with cdh23 but showed no evidence of a new complex peak (Figure S4A, D). When variants N1 and N2 of pcdh15 are combined to test the formation of a pseudo-heterophilic interaction, the results from SEC of the mixture indicate that a complex does not form (Figure 2B, orange). Variant N4 could not be combined with other pcdh15 variants due to its instability as noted above. Similarly, variants N5 and N6 were combined with each other, N1, and N2 and did not reveal formation of a complex (Figure S4B, E). Taken together, our experiments with the tips of PCDH15 suggest that PCDH15-PCDH15 bonds may involve pseudo-heterophilic combinations of variants we were unable to test (N3 or N4) or longer protein tips that extend beyond two EC repeats.

Structure of the cdh23-pcdh15(N2) Complex

To understand the interaction mediated by pcdh15(N2), we solved its crystal structure when bound to cdh23. The proteins remain arranged in an antiparallel, overlapping handshake with contacts formed between both EC repeats (Figure 3A). The structure of the complex reveals similarities and important differences to the canonical tip-link structure. Overall fold and quaternary arrangement are very similar. This is reflected in the low calculated backbone RMSD (<2 Å) between the cdh23-pcdh15(N1) complex (4AQ8) and the noncanonical cdh23-pcdh15(N2) complex (4XXW). The interface area between cdh23 and pcdh15(N2) is ~1100 $Å^2$, closely matching the canonical structure. Unlike variant N1, variant N2 of pcdh15 has a truncated N-terminus and is missing a canonical 3_{10} helix (Figure 3B). The intramolecular disulfide bond that clamps together EC1 and stabilizes the overall structure of the complex remains intact. The noncanonical structure still includes three calcium ions between EC1 and EC2 of both pcdh15(N2) and cdh23. This implies that the mechanical properties of each protomer remain similar as the binding of these calcium ions dictates the overall flexibility and elasticity of each protein.

Lining the interface between cdh23 and pcdh15(N2) are residues that are highly conserved and interact favorably. There are also several sites where deafness mutations are located at the protein-protein interface, and one in particular, PCDH15 R113G,[39] is found between the middle of EC1 of pcdh15 and the bottom of EC1 of cdh23. In the canonical structure, this residue is found pointing towards the interface (Figure 3C), whereas in the noncanonical structure R113 is pointing away from the interface (Figure 3D). The change in orientation of R113G is observed in both chains of pcdh15 found in the asymmetric unit of the cdh23-pcdh15(N2) complex. Importantly, this change in orientation results in the loss of both a salt bridge between residue R113 of pcdh15 and residue E77 of cdh23, and an intramolecular hydrogen bond between E77 and N96 of pcdh15.

Comparison of Binding Affinity Using SPR

To quantitatively characterize the noncanonical complex and the heterophilic interaction between pcdh15 and cdh23, the binding affinity between these two proteins was measured using SPR experiments at ambient temperature (25°C). Variants pcdh15(N1) or pcdh15(N2) were immobilized onto a gold chip modified with NTA by way of their hexahistidine tags. The analyte, cdh23 produced without an affinity tag, was then introduced onto the chip at concentrations ranging from 0-50 μM. The sensorgram was measured over 2 minutes, and the steady-state response was plotted as a function of concentration to calculate the binding affinity (K_d) (Figure 4A and B, Table 2). Based upon these measurements, the binding affinity of the canonical tip-link complex was 0.84 ± 0.03 μM (Figure 4A inset). The binding affinity of the noncanonical tip-link complex was 5.12 ± 0.30 μM (Figure 4B inset). This result quantitatively shows that pcdh15(N2) binds less strongly to cdh23 than the native N1 variant of pcdh15.

Comparison of Mechanical Strength *In Silico*

In addition to equilibrium binding affinity measurements, it is critical to understand how the tip-link complex will respond when a mechanical force is applied. During the sound transduction process, these proteins are capable of withstanding forces ranging from 10 to

100 pN.[40–42] The strength of the tip link can be probed *in silico* through the use of SMD simulations by pulling on the C-terminus of cdh23 and pcdh15 and observing complex dissociation. In this study, the mechanical strength of the canonical tip-link complex was compared with the noncanonical complex in duplicate SMD simulations at four different pulling speeds from 0.02 nm/ns to 10 nm/ns (Figure 5A and B). The constant velocity method was selected because it mimics, as closely as possible, the physiological stimulus of hearing. The results from all conditions tested revealed one main force peak (>350 pN) that corresponds with the unbinding of the tip-link complex. At all pulling velocities, the protein complex dissociated prior to any unfolding of the protein structure. This is clearly shown in snapshots of the noncanonical complex unbinding trajectory at different timepoints (marked with red arrows in Figure 5B) throughout a pulling simulation completed at 0.1 nm/ns (Figure 5C).

It is well known that the amount of force required to unbind a complex will decrease as the loading rate or pulling speed is decreased.[43, 44] Results from SMD simulations are most insightful at pulling speeds that approach or meet physiological hearing frequencies (10 kHz) and can be accomplished on reasonable computational timescales (hundreds of nanoseconds). The slowest pulling speed used in this study was 0.02 nm/ns (similar to physiological speeds of the basilar membrane reacting to high-frequency, loud sound[45]), and both systems showed the expected decrease in unbinding force as a function of decreasing pulling speed (Figure 5D). At the slowest velocities tested, 0.02 and 0.1 nm/ns, the average force required to dissociate the noncanonical complex was markedly lower (by 167 pN or 102 pN, respectively) than that required for the canonical complex (Figure 5D and Table S1) while at higher pulling speeds, 1 and 10 nm/ns, the average peak force values were closer in magnitude (26 or 41 pN, respectively). Closer examination of the trajectories reveals that the noncanonical complex dissociates at smaller forces when EC1 of cdh23 separates from EC2 of pcdh15. This is in contrast to the canonical complex where the repeats always remain in close contact throughout unbinding and instead slide apart (Figure S5). Taken together, the results from the SMD simulations support the experimental results that indicate the existence of a weaker noncanonical tip-link bond.

CONCLUSIONS

The diversity created by alternative splicing of PCDH15 leads to important biological questions surrounding the purpose of such structures in hearing, balance, and normal hair-cell function. Unfortunately, current antibodies are unable to distinguish variants N1-N6 in the ectodomain of PCDH15, therefore tracking when and where they appear in mechanosensitive hair cells remains a challenge. Our results clearly show that cdh23 and pcdh15(N1) form the most stable and mechanically strong tip link. For this reason, it is likely that this complex has been selected by the hair cell as the mature tip link, but it remains unclear why so many splice variants of PCDH15 remained through evolution. One consequence of creating alternative heterophilic tip links may be to tune the mechanical strength of the bond with CDH23. From this study, pcdh15(N2) results in a weaker tip-link interaction with cdh23, but it is possible that shortly after canonical tip-link disruption, for example due to exposure to loud sound, variant N2 may be enriched near the top of the stereocilia to form short-lived tip links while variant N1 is recruited to the proper position

for binding. We were unable to find evidence of a pseudo-heterophilic interaction between different pcdh15 variants. Therefore, PCDH15-PCDH15 links remain possible and may simply require the presence of additional EC repeats beyond the first two for binding to occur or may involve variants we were unable to test.

Current experimental evidence suggests that the tip link is a heterotetramer composed of one homodimer of PCDH15 and a second homodimer of CDH23.[3] Therefore, it is possible that different variants of PCDH15 may pair together as a dimer to bind in the same anti-parallel handshake manner to CDH23. If this were the case, then variant N1 and N2 of pcdh15 could form at least 3 different types of tip links each with its own set of unique binding affinities and nanomechanical properties. There are at least 5 options possible when considering all known variants of pcdh15 (Figure S6). The main challenge becomes identifying and understanding the physiological significance of each of these variants.

There is previous experimental evidence found in a wide range of organisms, which demonstrates that alternative splicing events can lead to functionally relevant proteins. One such example is Dscam, a gene that codes for a family of cell adhesion molecules that regulate neural wiring in *Drosophila melanogaster*. Stochastic alternative splicing of Dscam can theoretically produce up to 19,008 isoforms each with a distinct ectodomain and binding specificity.[46, 47] It is proposed that this level of complexity is required to provide each neuron a unique identity as each isoform has a strong preference for homophilic binding. In humans, neuroligin 1 (*NLGN1*) a protein located on the surface of neurons is an isoform specific ligand for neurexins. The splice isoforms of neuroligin 1 differentially regulate synaptogenesis.[48, 49] Both of these examples emphasize the importance of investigating each PCDH15 variant and understanding its binding behavior potentially encoding for heterotetrameric tip links of diverse mechanical strength. This could have significant implications in our understanding of hearing, tonotopy, and remodeling of tip links following sound-induced damage.

Supplementary Material

Refer to Web version on PubMed Central for supplementary material.

Acknowledgments

Simulations were performed at the Texas Advanced Computing Center (TACC)-Stampede, and the Ohio Supercomputer Center (OSC)-Oakley (PAS1037) supercomputers. Use of APS NE-CAT beamlines was supported by NIH (P41 GM103403 & S10 RR029205) and the Department of Energy (DE-AC02-06CH11357) through grant GUP 40277.

Funding Sources

This work was supported by The Ohio State University and by the National Institutes of Health, National Institute on Deafness and Other Communication Disorders (NIH NIDCD K99/R00 DC012534 and R01 DC015271). M.S. was an Alfred P. Sloan Fellow (FR-2015-65794).

ABBREVIATIONS

BAPTA 1,2-bis(*o*-aminophenoxy)ethane-*N,N,N′,N′*-tetraacetic acid

CDH23	cadherin 23
cdh23	cadherin 23 EC1-2
EC	extracellular cadherin
ITC	isothermal titration calorimetry
MALS	multi-angle light scattering
NTA	nitrilotriacetic acid
PCDH15	protocadherin 15
pcdh15	protocadherin 15 EC1-2
RMSD	root mean square deviation
SEC	size exclusion chromatography
SMD	steered molecular dynamics
SPR	surface plasmon resonance

References

1. Siemens J, Lillo C, Dumont RA, Reynolds A, Williams DS, Gillespie PG, Müller U. Cadherin 23 is a component of the tip link in hair-cell stereocilia. Nature. 2004; 428:950–955. [PubMed: 15057245]
2. Ahmed ZM, Goodyear RJ, Riazuddin S, Lagziel A, Legan PK, Behra M, Burgess SM, Lilley KS, Wilcox ER, Riazuddin S, Griffith AJ, Frolenkov GI, Belyantseva IA, Richardson GP, Friedman TB. The tip-link antigen, a protein associated with the transduction complex of sensory hair cells, is protocadherin-15. J Neurosci. 2006; 26:7022–7034. [PubMed: 16807332]
3. Kazmierczak P, Sakaguchi H, Tokita J, Wilson-Kubalek EM, Milligan RA, Müller U, Kachar B. Cadherin 23 and protocadherin 15 interact to form tip-link filaments in sensory hair cells. Nature. 2007; 449:87–91. [PubMed: 17805295]
4. Söllner C, Rauch GJ, Siemens J, Geisler R, Schuster SC, Müller U, Nicolson T, Consortium, T. S. Mutations in cadherin 23 affect tip links in zebrafish sensory hair cells. Nature. 2004; 428:955–959. [PubMed: 15057246]
5. Jaiganesh A, Narui Y, Araya-Secchi R, Sotomayor M. Beyond Cell-Cell Adhesion: Sensational Cadherins for Hearing and Balance. Cold Spring Harb Perspect Biol. 2017:a029280. [PubMed: 28847902]
6. Pickles JO, Comis SD, Osborne MP. Cross-links between stereocilia in the guinea pig organ of Corti, and their possible relation to sensory transduction. Hearing Res. 1984; 15:103–112.
7. Kachar B, Parakkal M, Kurc M, Zhao Y, Gillespie PG. High-resolution structure of hair-cell tip links. Proc Natl Acad Sci U S A. 2000; 97:13336–13341. [PubMed: 11087873]
8. Beurg M, Fettiplace R, Nam JH, Ricci AJ. Localization of inner hair cell mechanotransducer channels using high-speed calcium imaging. Nat Neurosci. 2009; 12:553–558. [PubMed: 19330002]
9. Hudspeth AJ, Corey DP. Sensitivity, polarity, and conductance change in the response of vertebrate hair cells to controlled mechanical stimuli. Proc Natl Acad Sci USA. 1977; 74:2407–2411. [PubMed: 329282]
10. Assad JA, Shepherd GM, Corey DP. Tip-link integrity and mechanical transduction in vertebrate hair cells. Neuron. 1991; 7:985–994. [PubMed: 1764247]
11. Zhao Y, Yamoah EN, Gillespie PG. Regeneration of broken tip links and restoration of mechanical transduction in hair cells. Proc Natl Acad Sci USA. 1996; 93:15469–15474. [PubMed: 8986835]

12. Indzhykulian AA, Stepanyan R, Nelina A, Spinelli KJ, Ahmed ZM, Belyantseva IA, Friedman TB, Barr-Gillespie PG, Frolenkov GI. Molecular remodeling of tip links underlies mechanosensory regeneration in auditory hair cells. PLoS Biol. 2013; 11:e1001583. [PubMed: 23776407]
13. Basu A, Lagier S, Vologodskaia M, Fabella BA, Hudspeth AJ. Direct mechanical stimulation of tip links in hair cells through DNA tethers. eLife. 2016; 5:e16041. [PubMed: 27331611]
14. Di Palma F, Holme RH, Bryda EC, Belyantseva IA, Pellegrino R, Kachar B, Steel KP, Noben-Trauth K. Mutations in Cdh23, encoding a new type of cadherin, cause stereocilia disorganization in waltzer, the mouse model for Usher syndrome type 1D. Nat Genet. 2001; 27:103–107. [PubMed: 11138008]
15. Alagramam KN, Murcia CL, Kwon HY, Pawlowski KS, Wright CG, Woychik RP. The mouse Ames waltzer hearing-loss mutant is caused by mutation of Pcdh15, a novel protocadherin gene. Nat Genet. 2001; 27:99–102. [PubMed: 11138007]
16. Bolz H, von Brederlow B, Ramirez A, Bryda EC, Kutsche K, Nothwang HG, Seeliger M, Cabrera M, Vila MC, Molina OP, Gal A, Kubisch C. Mutation of CDH23, encoding a new member of the cadherin gene family, causes Usher syndrome type 1D. Nat Genet. 2001; 27:108–112. [PubMed: 11138009]
17. Bork JM, Peters LM, Riazuddin S, Bernstein SL, Ahmed ZM, Ness SL, Polomeno R, Ramesh A, Schloss M, Srisailpathy CR, Wayne S, Bellman S, Desmukh D, Ahmed Z, Khan SN, Kaloustian VM, Li XC, Lalwani A, Riazuddin S, Bitner-Glindzicz M, Nance WE, Liu XZ, Wistow G, Smith RJ, Griffith AJ, Wilcox ER, Friedman TB, Morell RJ. Usher syndrome 1D and nonsyndromic autosomal recessive deafness DFNB12 are caused by allelic mutations of the novel cadherin-like gene CDH23. Am J Hum Genet. 2001; 68:26–37. [PubMed: 11090341]
18. Brasch J, Harrison OJ, Honig B, Shapiro L. Thinking outside the cell: how cadherins drive adhesion. Trends Cell Biol. 2012; 22:299–310. [PubMed: 22555008]
19. Hirano S, Takeichi M. Cadherins in brain morphogenesis and wiring. Physiol Rev. 2012; 92:597–634. [PubMed: 22535893]
20. Furness DN, Hackney CM. Cross-links between stereocilia in the guinea pig cochlea. Hearing Res. 1985; 18:177–188.
21. Furness DN, Katori Y, Nirmal Kumar B, Hackney CM. The dimensions and structural attachments of tip links in mammalian cochlear hair cells and the effects of exposure to different levels of extracellular calcium. Neuroscience. 2008; 154:10–21. [PubMed: 18384968]
22. Sotomayor M, Weihofen WA, Gaudet R, Corey DP. Structure of a force-conveying cadherin bond essential for inner-ear mechanotransduction. Nature. 2012; 492:128–132. [PubMed: 23135401]
23. Geng R, Sotomayor M, Kinder KJ, Gopal SR, Gerka-Stuyt J, Chen DHC, Hardisty-Hughes RE, Ball G, Parker A, Gaudet R, Furness D, Brown SD, Corey DP, Alagramam KN. Noddy, a Mouse Harboring a Missense Mutation in Protocadherin-15, Reveals the Impact of Disrupting a Critical Interaction Site between Tip-Link Cadherins in Inner Ear Hair Cells. J Neurosci. 2013; 33:4395–4404. [PubMed: 23467356]
24. Goodyear RJ, Richardson GP. A Novel Antigen Sensitive to Calcium Chelation That is Associated with the Tip Links and Kinocilial Links of Sensory Hair Bundles. J Neurosci. 2003; 23:4878–4887. [PubMed: 12832510]
25. Goodyear RJ, Forge A, Legan PK, Richardson GP. Asymmetric distribution of cadherin 23 and protocadherin 15 in the kinocilial links of avian sensory hair cells. J Comp Neurol. 2010; 518:4288–4297. [PubMed: 20853507]
26. Webb SW, Grillet N, Andrade LR, Xiong W, Swarthout L, Della Santina CC, Kachar B, Müller U. Regulation of PCDH15 function in mechanosensory hair cells by alternative splicing of the cytoplasmic domain. Development. 2011; 138:1607–1617. [PubMed: 21427143]
27. Pepermans E, Michel V, Goodyear R, Bonnet C, Abdi S, Dupont T, Gherbi S, Holder M, Makrelouf M, Hardelin JP, Marlin S, Zenati A, Rhichardson G, Avan P, Bahloul A, Petit C. The CD2 isoform of protocadherin-15 is an essential component of the tip-link complex in mature auditory hair cells. EMBO Mol Med. 2014; 6:984–992. [PubMed: 24940003]
28. Tsumoto K, Shinoki K, Kondo H, Uchikawa M, Juji T, Kumagai I. Highly efficient recovery of functional single-chain Fv fragments from inclusion bodies overexpressed in Escherichia coli by

controlled introduction of oxidizing reagent–application to a human single-chain Fv fragment. J Immunol Methods. 1998; 219:119–129. [PubMed: 9831393]

29. Otwinowski Z, Minor W. Processing of X-ray diffraction data collected in oscillation mode. Methods Enzymol. 1997; 276:307–326.
30. McCoy AJ, Grosse-Kunstleve RW, Adams PD, Winn MD, Storoni LC, Read RJ. Phaser crystallographic software. J Appl Crystallogr. 2007; 40:658–674. [PubMed: 19461840]
31. Emsley P, Cowtan K, IUCr. Coot: model-building tools for molecular graphics. Acta Crystallogr Sect D: Biol Crystallogr. 2004; 60:2126–2132. [PubMed: 15572765]
32. Murshudov GN, Skubák P, Lebedev AA, Pannu NS, Steiner RA, Nicholls RA, Winn MD, Long F, Vagin AA. REFMAC5 for the refinement of macromolecular crystal structures. Acta Crystallogr., Sect D: Biol Crystallogr. 2011; 67:355–367. [PubMed: 21460454]
33. Karplus M, Petsko GA. Molecular dynamics simulations in biology. Nature. 1990; 347:631–639. [PubMed: 2215695]
34. Sotomayor M, Schulten K. Single-molecule experiments in vitro and in silico. Science. 2007; 316:1144–1148. [PubMed: 17525328]
35. Humphrey W, Dalke A, Schulten K. VMD: visual molecular dynamics. J Mol Graph. 1996; 14:33–38. 27–38. [PubMed: 8744570]
36. Phillips JC, Braun R, Wang W, Gumbart J, Tajkhorshid E, Villa E, Chipot C, Skeel RD, Kalé L, Schulten K. Scalable molecular dynamics with NAMD. J Comput Chem. 2005; 26:1781–1802. [PubMed: 16222654]
37. Huang J, MacKerell AD. CHARMM36 all-atom additive protein force field: validation based on comparison to NMR data. J Comput Chem. 2013; 34:2135–2145. [PubMed: 23832629]
38. Araya-Secchi R, Neel BL, Sotomayor M. An elastic element in the protocadherin-15 tip link of the inner ear. Nat Commun. 2016; 7:13458. [PubMed: 27857071]
39. Ahmed ZM, Riazuddin S, Ahmad J, Bernstein SL, Guo Y, Sabar MF, Sieving P, Riazuddin S, Griffith AJ, Friedman TB, Belyantseva IA, Wilcox ER. PCDH15 is expressed in the neurosensory epithelium of the eye and ear and mutant alleles are responsible for both USH1F and DFNB23. Hum Mol Genet. 2003; 12:3215–3223. [PubMed: 14570705]
40. Cheung E, Corey DP. Ca2+ changes the force sensitivity of the hair-cell transduction channel. Biophys J. 2006; 90:124–139. [PubMed: 16214875]
41. Howard J, Hudspeth AJ. Compliance of the hair bundle associated with gating of mechanoelectrical transduction channels in the bullfrog's saccular hair cell. Neuron. 1988; 1:189–199. [PubMed: 2483095]
42. Jaramillo F, Hudspeth AJ. Displacement-clamp measurement of the forces exerted by gating springs in the hair bundle. Proc Natl Acad Sci USA. 1993; 90:1330–1334. [PubMed: 7679501]
43. Bell GI. Models for the specific adhesion of cells to cells. Science. 1978; 200:618–627. [PubMed: 347575]
44. Evans E, Ritchie K. Dynamic strength of molecular adhesion bonds. Biophys J. 1997; 72:1541–1555. [PubMed: 9083660]
45. Robles L, Ruggero MA. Mechanics of the mammalian cochlea. Physiol Rev. 2001; 81:1305–1352. [PubMed: 11427697]
46. Wojtowicz WM, Flanagan JJ, Millard SS, Zipursky SL, Clemens JC. Alternative splicing of Drosophila Dscam generates axon guidance receptors that exhibit isoform-specific homophilic binding. Cell. 2004; 118:619–633. [PubMed: 15339666]
47. Wojtowicz WM, Wu W, Andre I, Qian B, Baker D, Zipursky SL. A Vast Repertoire of Dscam Binding Specificities Arises from Modular Interactions of Variable Ig Domains. Cell. 2007; 130:1134–1145. [PubMed: 17889655]
48. Ichtchenko K, Hata Y, Nguyen T, Ullrich B, Missler M, Moomaw C, Südhof TC. Neuroligin 1: A splice site-specific ligand for β-neurexins. Cell. 1995; 81:435–443. [PubMed: 7736595]
49. Boucard AA, Chubykin AA, Comoletti D, Taylor P, Südhof TC. A Splice Code for trans-Synaptic Cell Adhesion Mediated by Binding of Neuroligin 1 to α- and β-Neurexins. Neuron. 2005; 48:229–236. [PubMed: 16242404]

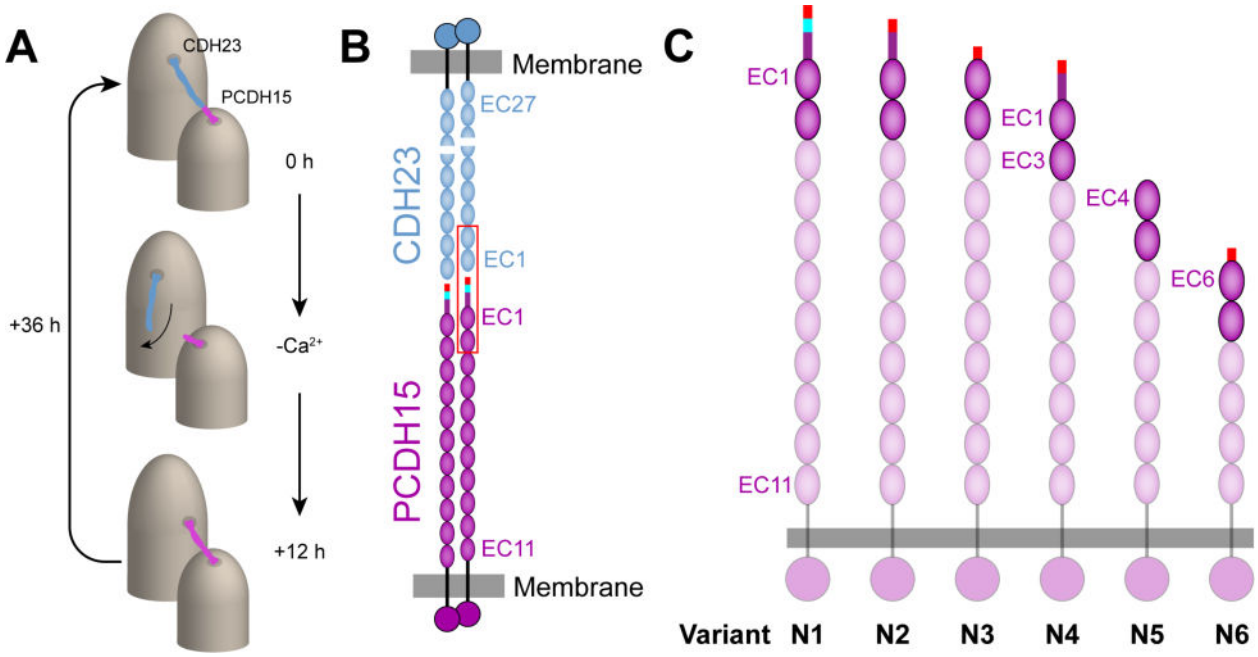

Figure 1.

Model of the tip link interaction and structural details of the splice variants of PCDH15. (A) The tip link is composed of CDH23 and PCDH15 and connects adjacent stereocilia located on the apical side of hair cells. Upon removal of calcium, the tip link is disrupted and forms short-lived PCDH15-PCDH15 links.[12] (B) Each homodimer of CDH23 and PCDH15 bind together to form an antiparallel heterotetrameric complex. The first two EC repeats located at the N-terminus of each protein form a mechanically strong bond (outlined in red). (C) PCDH15 is present in at least 26 alternative splice variants, and a subset of these variants has alterations in the first two EC repeats (opaque ovals). These variants have been grouped into 6 categories numbered N1-N6 (Figure S1). The start of the N-terminus is drawn as a rectangle where the end of exon 2 is indicated in red, exon 3 is shown in cyan, and exon 4 is shown in purple.

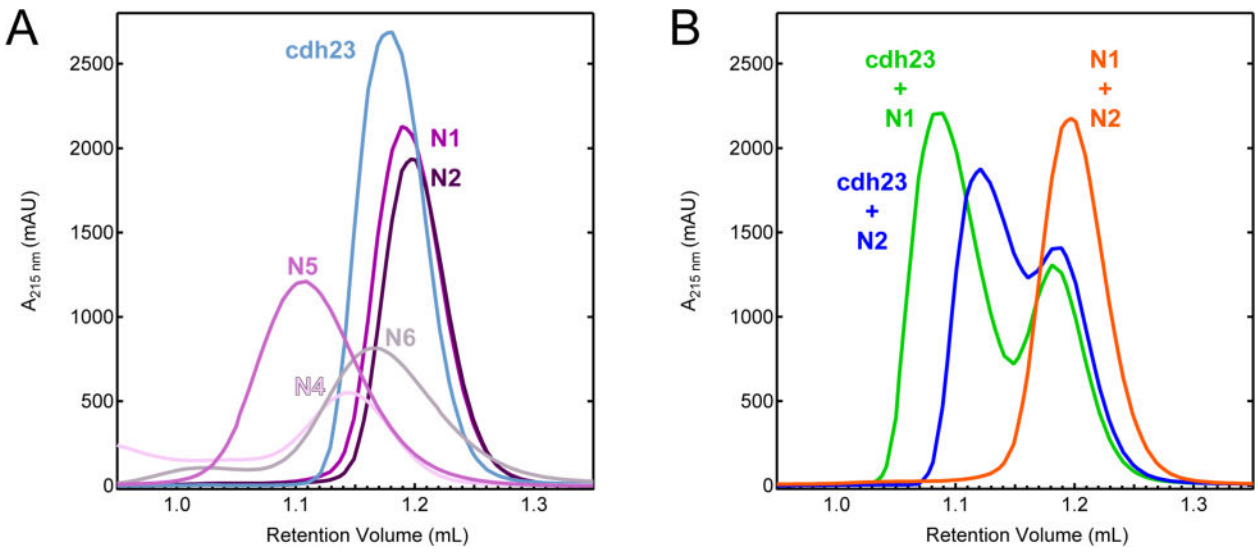

Figure 2.

Analytical SEC analysis of pcdh15 variants and complexes. (A) Chromatograms of individual cdh23 and pcdh15 variants. (B) Mixtures of cdh23 and pcdh15. Formation of heterophilic tip link complexes is noted by the presence of a second peak in the trace.

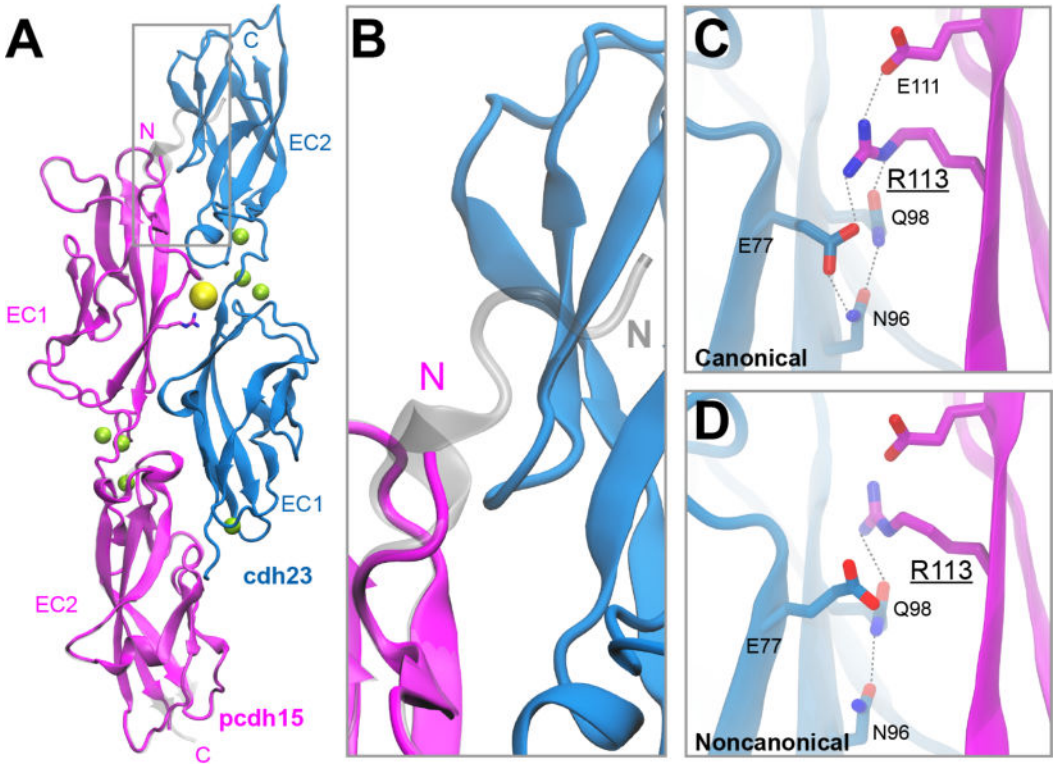

Figure 3.

Structure of a noncanonical cdh23-pcdh15 complex. (A) X-ray crystal structure of cdh23 and pcdh15(N2) (PDB: 4XXW) overlaid with the canonical cdh23 and pcdh15(N1) (PDB: 4AQ8) complex (shown in gray). (B) Region of gray box in panel (A), highlighting important structural differences at the N-terminus of pcdh15. (C) Detail of the interface between cdh23 and pcdh15 shows residue R113 pointing towards the interface in the canonical structure. (D) In the noncanonical structure, R113 is oriented away from the interface and forms fewer favorable interactions with nearby residues.

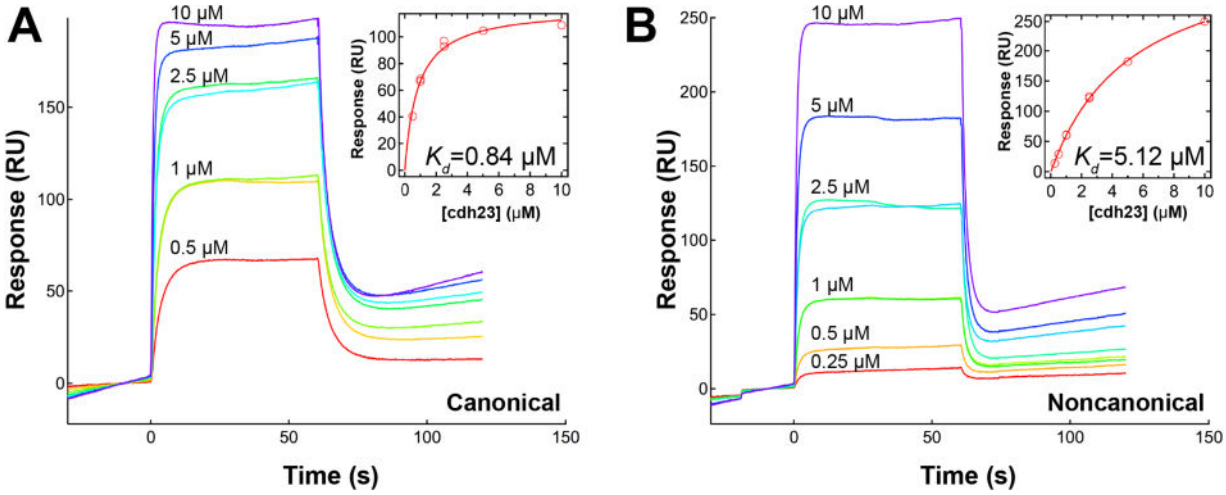

Figure 4.

Measurement of cdh23-pcdh15 binding affinity by SPR. (A) Raw sensorgrams of binding between cdh23 at varying concentrations with immobilized pcdh15(N1). Inset plot shows peak response as a function of cdh23 concentration. K_d is 0.84 ± 0.03 μM for the canonical complex. (B) Sensorgrams for binding of cdh23 to pcdh15(N2) with a measured K_d of 5.12 ± 0.30 μM.

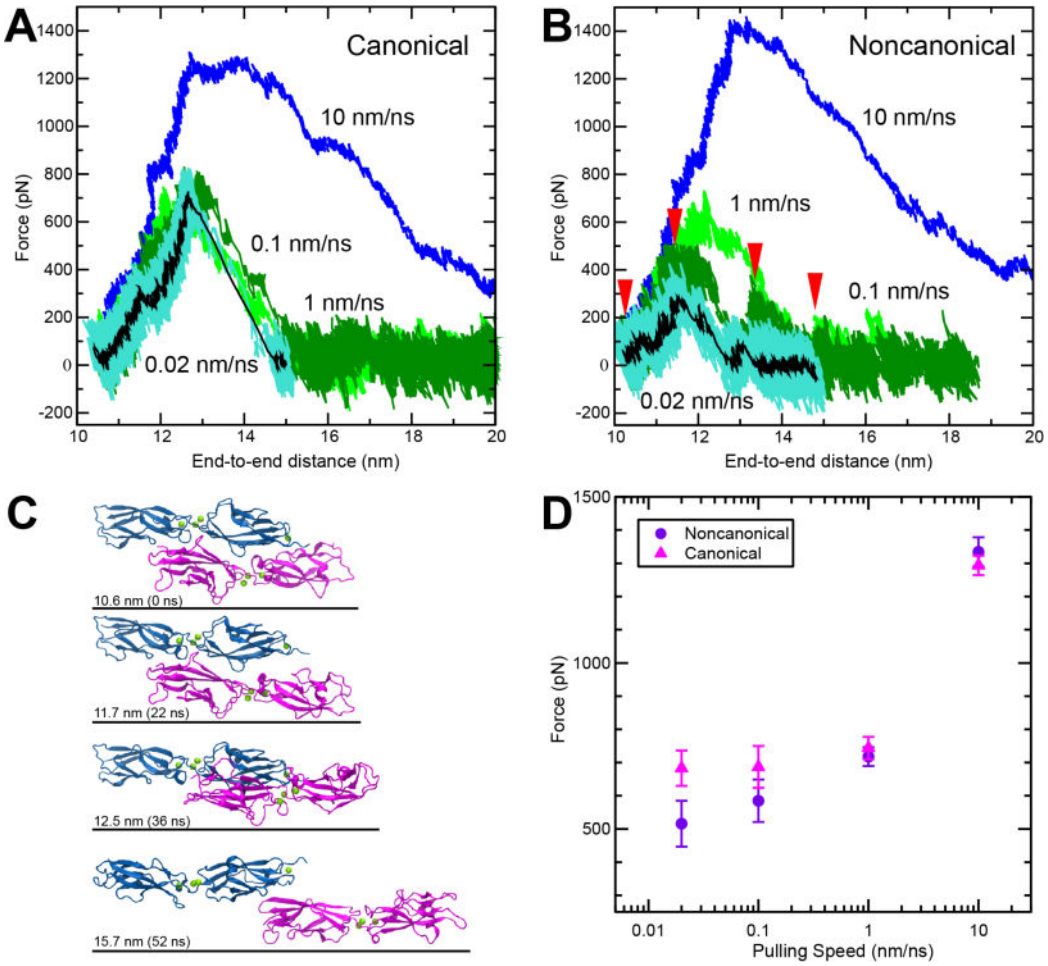

Figure 5.

SMD simulations predict that the complex formed by cdh23 and pcdh15(N2) can be weaker than the complex formed with pcdh15(N1). (A-B) Force vs. end-to-end distance for (A) canonical complex formed by cdh23 and pcdh15(N1) (simulations S3b to S3e, Table S1) and (B) noncanonical complex formed by cdh23 and pcdh15(N2) (simulations S1b to S1e) at pulling speeds of 10 nm/ns (blue); 1 nm/ns (light green); 0.1 nm/ns (dark green); and 0.02 nm/ns (cyan; running average of 1 ns in black). (C) Snapshots from simulation S1d (0.1 nm/ns; Table S1) during unbinding at timepoints indicated by red arrows in (B). (D) Plot of average peak force vs. pulling speed for both variants (Table S1). Bars represent the standard error.

Table 1

Data Collection and Refinement Statistics for the Crystal Structure of cdh23 and pcdh15(N2)

Data Collection and Refinement	
Space group	C121
Unit cell parameters:	
a, b, c (Å)	157.75, 57.79, 155.26
α,β,γ (°)	90, 99.17, 90
Molecules per asymmetric unit	2
Beam source	APS 24-ID-C
Wavelength (Å)	0.97920
Resolution limit (Å)	2.26
Unique reflections	65061 (2736)
Redundancy	3.2 (2.5)
Completeness (%)	96.8 (84.9)
Average I/σ(I)	13.4 (2.3)
R_{merge}	0.08 (0.40)
Refinement	
Resolution Range (Å)	50.0-2.26 (2.30-2.26)
Residues (atoms)	866 (6790)
Water molecules	463
R_{work} (%)	18.7 (28.4)
R_{free} (%)	23.3 (35.2)
RMS deviations	
Bond lengths (Å)	0.018
Bond angles (°)	1.806
B-factor average	
Protein	54.3
Ligand/ion	39.1
Water	44.9
Ramachandran Plot Regions	
Most favored (%)	88.9

Data Collection and Refinement	
Additionally allowed (%)	10.7
Generously allowed (%)	0.4
Disallowed (%)	0.0
Interface Area (Å^2)	1102.3
PDB ID code	4XXW

Table 2

Summary of Binding Affinity Measurements of cdh23 and pcdh15 Complexes Using Different Experimental Methods and Conditions.

	Method	Temperature (°C)	(μM)
cdh23 + pcdh15(N1)[22]	ITC	10	2.9 ± 0.4
cdh23 + pcdh15(N1)	SPR	25	0.84 ± 0.03, $n = 2$
cdh23 + pcdh15(N2)	SPR	25	5.12 ± 0.30, $n = 2$